Electronic Supplementary Material (ESI) for Journal of Materials Chemistry A.

Knitting Aryl Network Polymers (KAPs) Embedded Copper Foam Enables Highly Efficient Thermal Energy Storage

Changhui Liu, [a] Jianhua Zong, [a] Jiahao Zhang, [a] Deqing He, [a] Chenglong Guo, [a] Ben Xu[b] and Zhonghao Rao *[a]

[a] Laboratory of Energy Storage and Heat Transfer, School of Electrical and Power Engineering, China University of Mining and Technology, Xuzhou, 221116, China. Email: raozhonghao@cumt.edu.cn

[b] Department of Mechanical Engineering, University of Texas Rio Grande Valley, Edinburg, TX 78539, USA.

Note 1: A typical preparation procedure of KAPs-CF-PCM

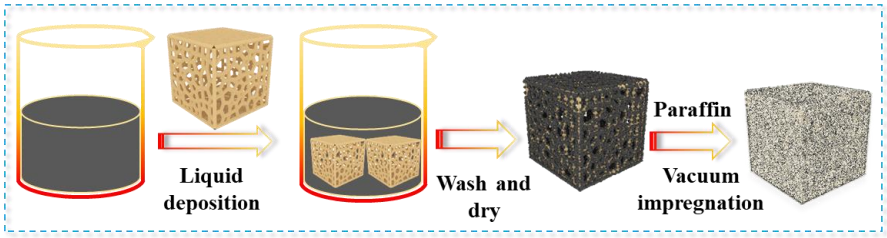

The preparation was conducted in a 100 mL beaker, benzene (1.56 g, 0.02 mol) was mixed with triphenylphosphine (5.25 g, 0.02 mmol), anhydrous $FeCl_3$ (9.75 g, 0.06 mol) and DCE (20 mL) at 45 °C. Copper foam (20 mm × 20 mm × 20 mm, ca. 1.2 g) was put in the reaction mixture after the starting materials dissolved in the solvent completely. Subsequently, formaldehyde dimethyl acetal (FDA) (4.56 g, 0.06 mol) was added, the reaction mixture was then allowed to heat at 80 °C to initiate the reaction and kept that temperature for 60 h. Polymer embedded copper foam was taken out and rinsed with anhydrous MeOH for several times after the completion of reaction. After drying in a vacuum oven at 60 °C for 6 h, the polymer embedded copper foam was submitted to a vacuum impregnation of paraffin. The final KAPs-CF-PCM was obtained after being heated at 80 °C with the aim of the removal of the surficial unadsorbed paraffin wax.

A typical preparation procedure of KAPs-PCM

KAPs was prepared using the similar procedure with that of KAPs-CF-PCM in the absence of opper foam. KAPs-PCM was then obtained by blending paraffin (10 g) and KAPs (2.5 g) under a vacuum condition.

Note 2: Calculation method of the encapsulation rate.

Because copper foam cannot contribute latent heat, measured latent heat containing a copper foam component may bring a large error due to the extreme tiny amount of the measured sample, so the latent heat of KAPs-CF-PCM is calculated based on Eq. S1, subsequently, the encapsulation rate can be obtained using Eq. S2,

$$\Delta \boldsymbol{H}_{\mathrm{s}} = \frac{(\boldsymbol{m_1}-\boldsymbol{m_2})*\Delta \boldsymbol{H}_{s1}}{\boldsymbol{m_1}} \quad \text{(Eq. S1)}$$

$$\boldsymbol{\eta} = \frac{\Delta \boldsymbol{H}_{s}}{\Delta \boldsymbol{H}_{p}} \quad \text{(Eq. S2)}$$

Where ΔH_s is the latent heat of KAPs-CF-PCM, m_1 is assigned to the weight of the final obtained PCM composite, m_2 is the weight of the starting copper foam, ΔH_{s1} means the measured melting latent heat of KAPs-CF-PCM after removing copper skeleton, and η represents the encapsulation rate ΔH_p corresponds to the melting latent heat of pristine paraffin wax.

Note 3: Calculation of thermal conductivity.

The thermal conductivity of KAPs-CF-PCM is measured by sandwiching the material between a cool source (ice-water bath) at 10 °C and an electrical heating plate (4×4 cm) with tunable heating power. and the thermocouples was placed on top surface and the bottom surface. The whole structure was monitored by Date acquisition (Keysight 34970A, made by USA), after the power of DC power supply was turned on, a range of temperature gradients would exhibit across the sandwich. The thermal couductivity can be calculated by the Fourier equation, given the heat flux and the temperature gradient in the material.

$$Q = A\mathrm{k}\frac{\Delta T}{\Delta X} + Q_{\mathrm{loss}}$$

where A is the top surface area of the sample, ΔT/Δx is the temperature gradient between the top surface and the bottom surface, and Q_{loss} is the heat loss from the heat source to environment. Through linearly fitting the measured data points under different heating power inputs, the thermal conductivity of the KAPs-CF-PCM heat sink was estimated up to 55.37 W/m K.

KAPs-CF-PCM(2)

Power/W	**Top_{avg}/°C**	**$Bottom_{avg}$/°C**	**ΔT_1/°C**	**ΔT_2/°C**	**ΔT_3/°C**
0.218	16.628	12.701	4.313	4.875	3.750
0.46	21.701	13.516	9.027	10.367	7.687
0.988	31.908	15.249	18.434	21.228	15.639
1.591	43.354	17.216	29.035	34.134	23.936
2.293	57.086	16.800	39.848	40.139	39.556
3.402	75.625	18.826	56.252	56.471	56.032
4.213	88.574	23.412	64.440	63.179	65.700
5.141	109.966	27.314	83.815	86.821	80.809
0.134	15.037	13.925	2.533	2.709	2.356
0.530	24.236	15.008	10.457	11.092	9.821

CF

Power/W	**Top_{avg}/°C**	**$Bottom_{avg}$/°C**	**ΔT_1/°C**	**ΔT_2/°C**	**ΔT_3/°C**
0.267	17.673	14.430	5.065	6.467	3.662
0.665	26.512	15.538	12.984	16.453	9.514

1.210	38.264	16.614	23.638	30.029	17.246
1.665	47.538	16.930	31.830	40.116	23.543
2.420	62.159	18.461	44.686	56.066	33.306
3.267	77.780	19.128	58.214	72.822	43.605
3.823	86.805	20.315	66.599	84.295	48.903

P_1=UI, and the P_1 due to the DC power supply. Because the sample is Covered by foam which is simplified as a adiabatic environment, and top area of sample is 2×2 cm, the electrical heating plate is 4×4 cm, so P_2=1/4 P_1, P_2 is known as the real heating power, so the numerical value of $\triangle T/ P_2$ is the method to evaluation sample's thermal conductivity.

Note 4: Calculation method of the Light-to-thermal conversion efficiency.

Light-to-thermal conversion efficiency (η) of KAPs-CF-PCM was estimated according to the ratio of heat stored in the composite with respect to the light energy stored by sample during the phase change process. By referring literatures [1] , Eq. (S3) was used to calculate the value of η,

$$\eta = \frac{m\Delta H_c}{\rho S(t_f - t_s)} \quad \text{(Eq. S3)}$$

where m is the mass of the KAPs-CF-PCM composite, $\triangle H_c$ represents the phase change enthalpy obtained from DSC result, ρ is intensity of the simulant light source, t_f and t_s are the light driven phase change time of the sample before and after phase change, respectively.

m/g	S/cm^2	$t_f - t_s$/s	ρ/mW·cm^{-2}	η
3.625	3.8	1074	100	93.8%

Figure S1 Photographs of copper foams with different pore density (porosity per inch, PPI) in the same porosity of 98%.

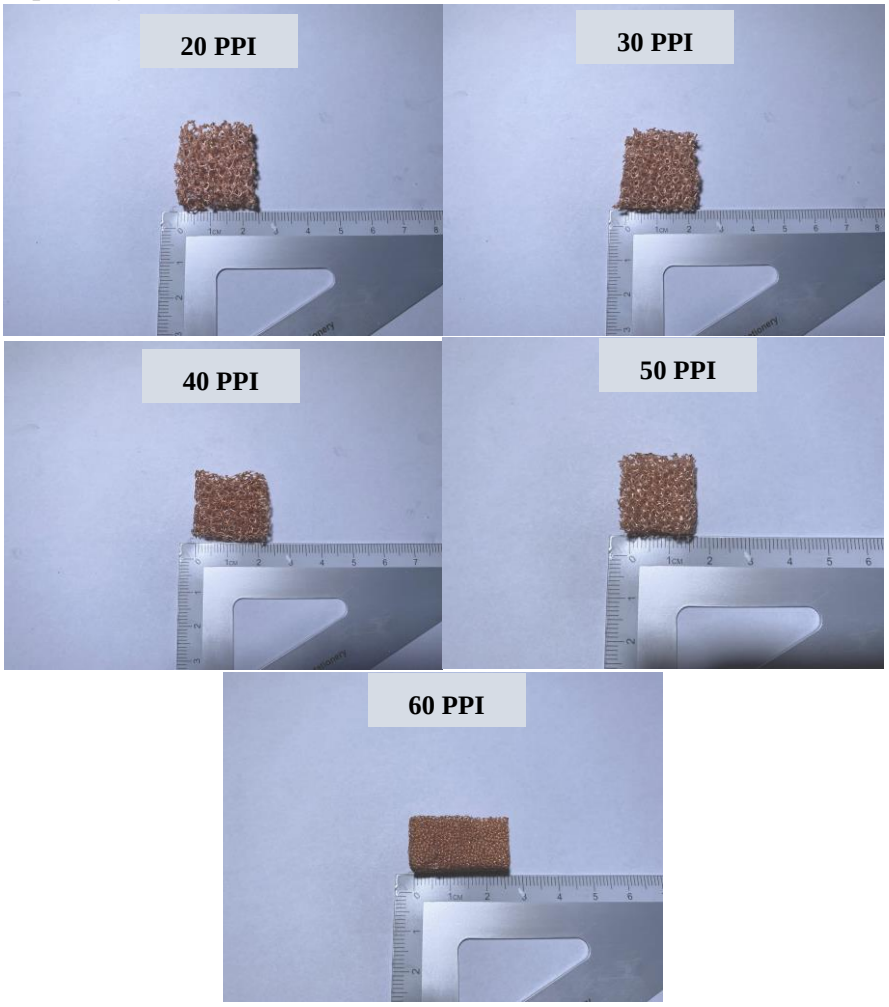

Table S1 Study on the different reaction parameters.[a]

Sample	PPI	DCE (mL)	ΔH_s (J/g)	Encapsulation rate (%)
KAPs-CF-PCM (**1**)	20	20	70.94	41.7
KAPs-CF-PCM (2)	**30**	**20**	**105.50**	**62.1**
KAPs-CF-PCM (**3**)	40	20	68.67	40.4
KAPs-CF-PCM (**4**)	50	20	79.51	46.8
KAPs-CF-PCM (**5**)	60	20	74.28	43.7
KAPs-CF-PCM (**6**)	20	40	68.85	40.5
KAPs-CF-PCM (**7**)	30	40	64.76	38.1
KAPs-CF-PCM (**8**)	40	40	78.78	46.3
KAPs-CF-PCM (**9**)	50	40	96.40	56.7
KAPs-CF-PCM (**10**)	60	40	63.96	37.6
KAPs-CF-PCM (**11**)	30	15	55.96	32.9
KAPs-CF-PCM (**12**)[b]	30	20	48.56	28.6
KAPs-CF-PCM (**13**)[c]	30	20	35.32	20.8

[a] Unless otherwise noted, the reaction condition is as following: benzene (1.56 g, 0.02 mol), triphenylphosphine (5.25 g, 0.02 mmol), FDA (4.56 g, 0.06 mol), DCE (20 mL) copper foam (20 mm × 20 mm × 20 mm, ca. 1.2 g), at 80 °C for 60 h.[b] benzene (3.12 g, 0.04 mol), FDA (4.56 g, 0.06 mol), DCE (20 mL) copper foam (20 mm × 20 mm × 20 mm, ca. 1.2 g), at 80 °C for 60 h. [c] benzene (1.56 g, 0.02 mol), 1, 3, 5-triphenylbenzene (6.12 g, 0.02 mmol), FDA (4.56 g, 0.06 mol), DCE (20 mL) copper foam (20 mm × 20 mm × 20 mm, ca. 1.2 g), at 80 °C for 60 h.

In order to understand the effect of pore density on the encapsulation rate of this polymer embedding copper foam, a series of copper foams bearing different pore density with the same porosity were employed to study. As it is shown in Table S1, copper foam with a pore density of 30 PPI affords the outstanding encapsulation efficiency, which means that neither too big nor small pore in copper

foam could lead to a good performance. We suspect that the reason might be dominated by two factors, on the one hand, low pore density would result in a relatively big hole among the rigid copper skeleton, which would thus lead to the decrease amount of polymer embedding and consequently a decline in the encapsulation of paraffin. On the other hand, a high density of pore in the copper foam hampers the penetration of starting materials in the chamber of copper foam, which is also a negative factor for the downstream growth of polymer on the copper foam skeleton and thus leads to the poor encapsulation performance of paraffin. Therefore, an appropriate pore density is a key factor for the growth of polymer on the skeleton of copper foam. In addition, we also paid attention on the reaction solution concentration since it will not only impact the final proportion of polymer in KAPs-CF materials, but also associate with the dynamic of polymerization process because a concentrated reaction solution might afford a rapid polymerization on the surface of copper foam and this formed polymer will block the deep growth of polymer inside the copper foam. Based on the results obtained and this analysis, we found that 30 PPI and 2 M are the optimal pore density and reaction concentration respectively.

Figure S2 SEM image of KAPs prepared in the absence copper foam.

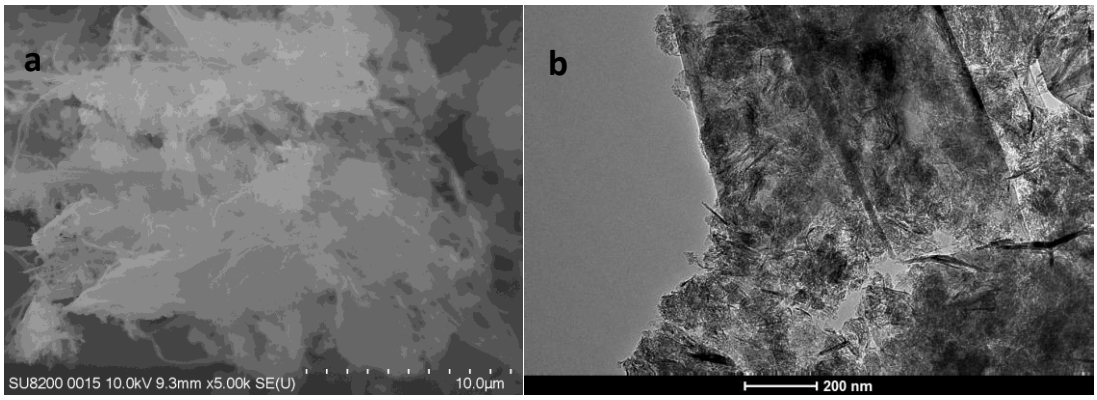

Figure S3 High resolution TEM image of KAPs-CF.

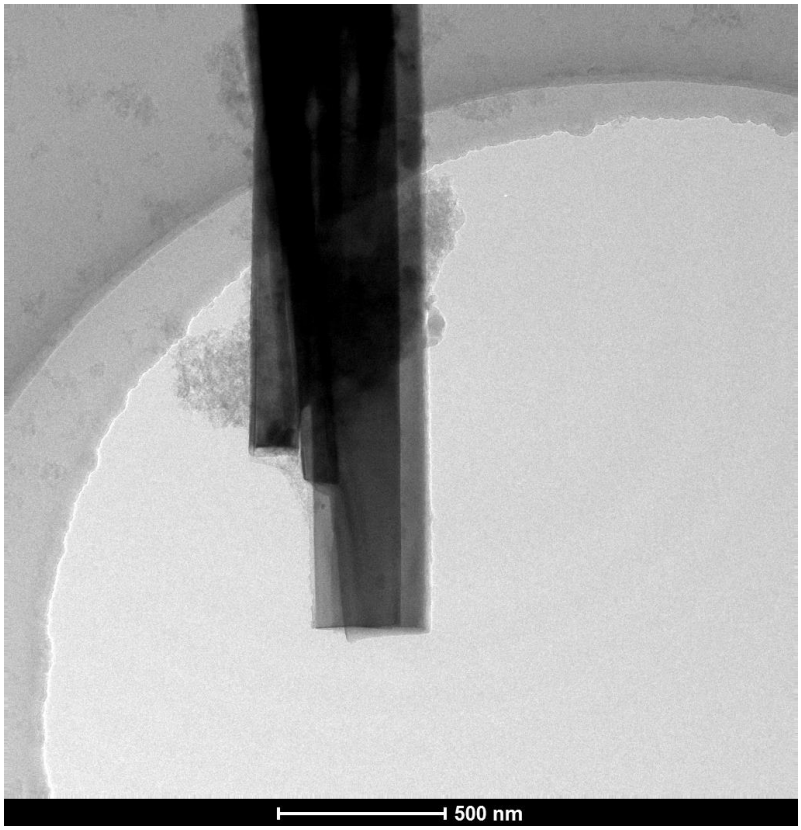

Figure S4 Characterization of KAPs-CF-PCM (12). (a) SEM, (b) TEM image of KAPs-CF (12), (c) XRD, (d) FTIR spectra of KAPs-CF-PCM (12), (e) XPS survey, (f) C 1s of KAPs-CF-PCM (12).

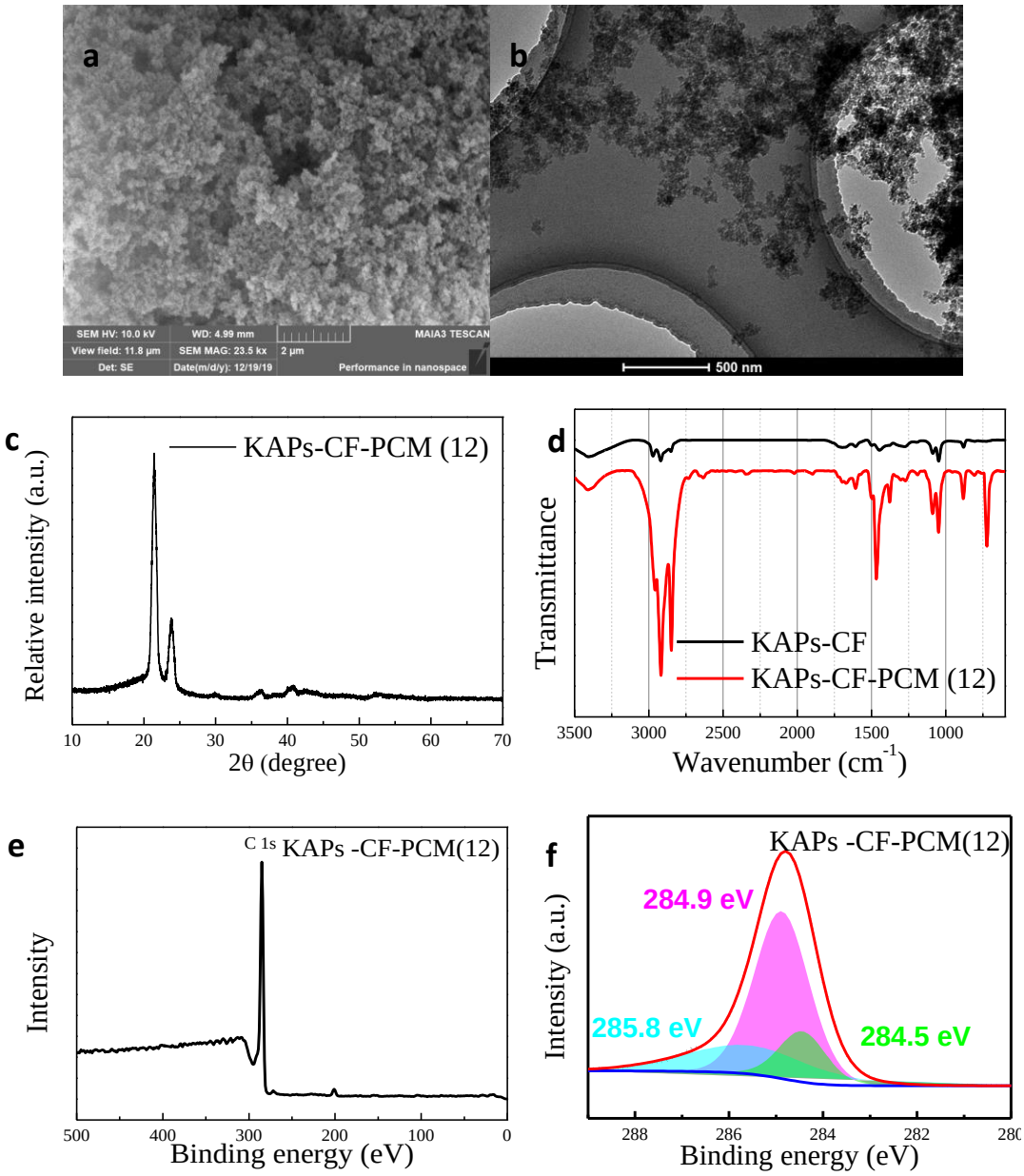

Figure S5 Characterization of KAPs-CF-PCM (13), (a) SEM, (b) TEM image of KAPs-CF (13), (c) XRD, (d) FTIR spectra of KAPs-CF-PCM (13), (e) XPS survey, (f) C 1s of KAPs-CF-PCM (13).

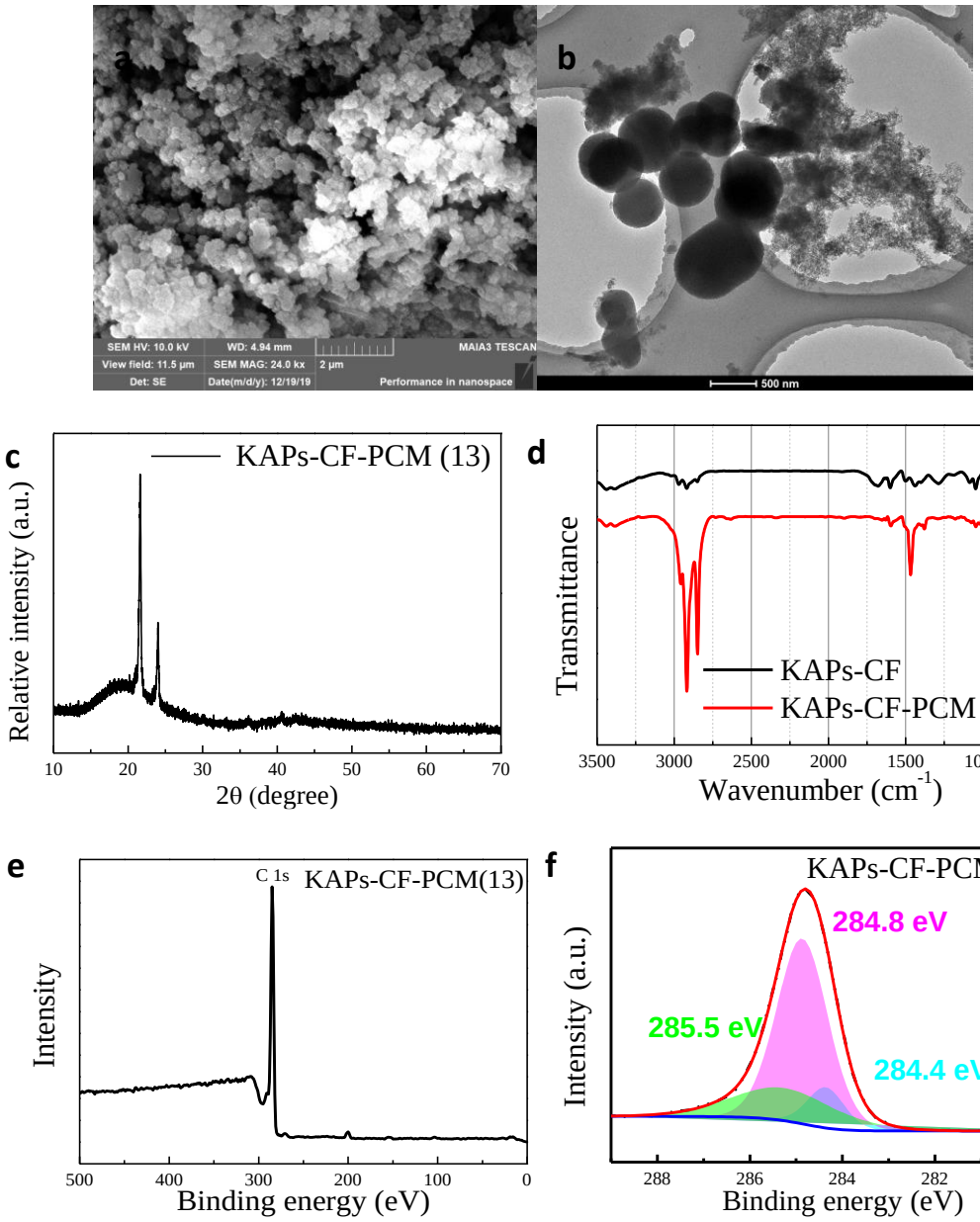

Figure S6 N_2 adsorption-desorption isotherms patterns (a), and pore size distribution (b) of KAPs-CF (12).

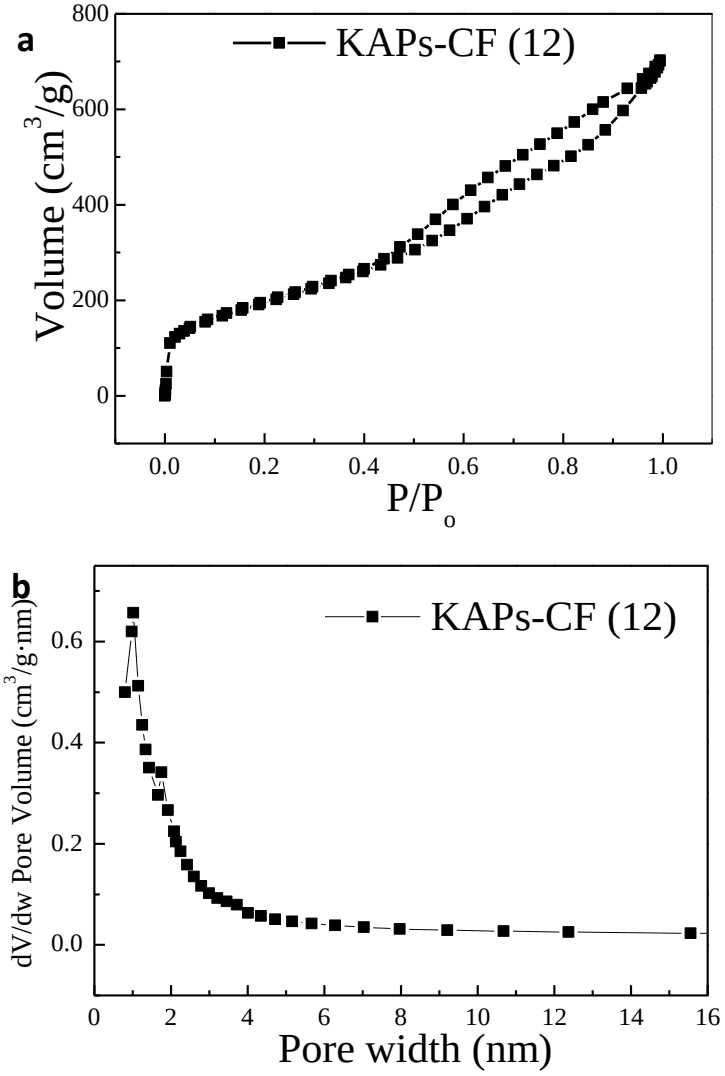

Figure S7 N_2 adsorption-desorption isotherms patterns (a), and pore size distribution (b) of KAPs-CF (13).

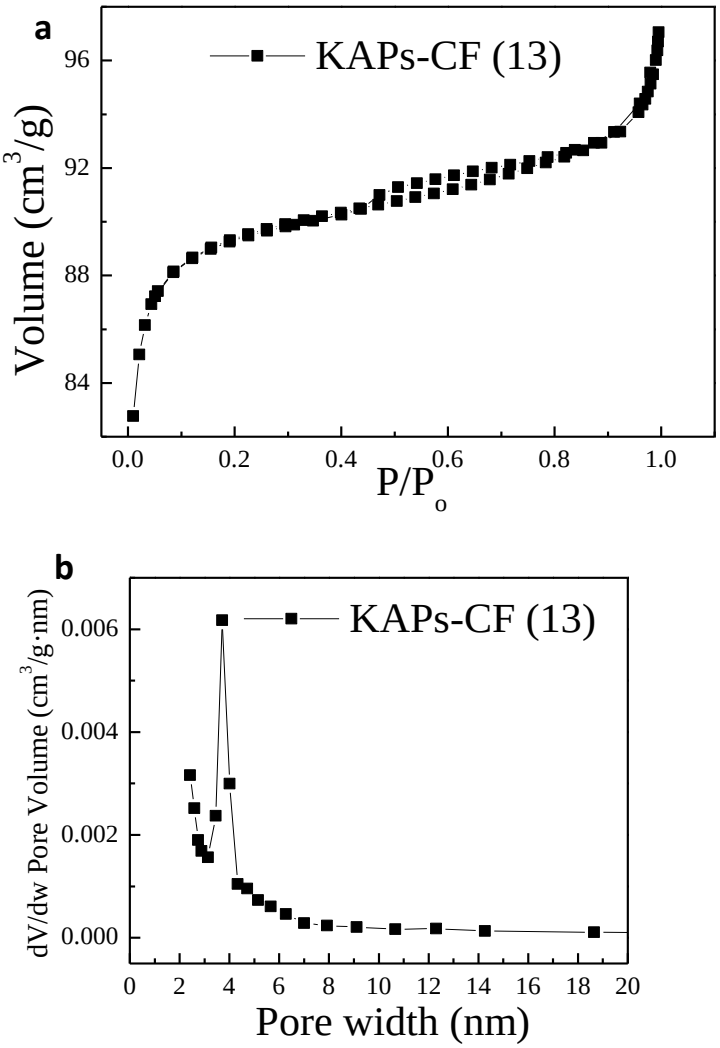

Figure S8 (a) Photograph of thermal conductivity testing platform and (b) schematic illustration of thermal conductivity measurement platform.

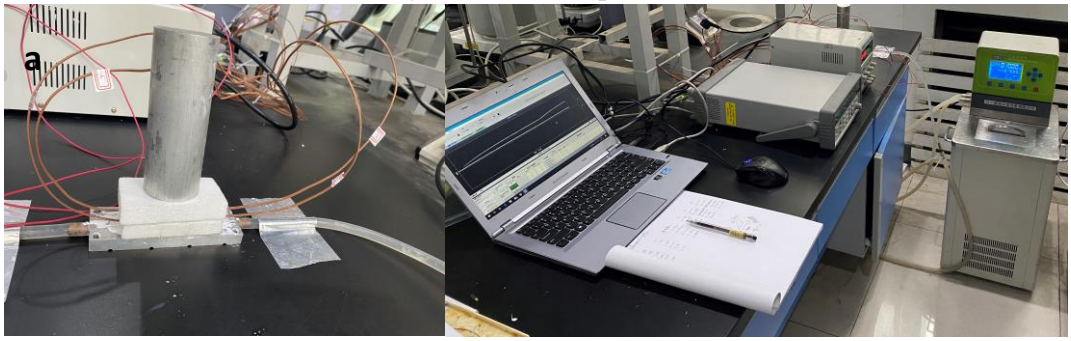

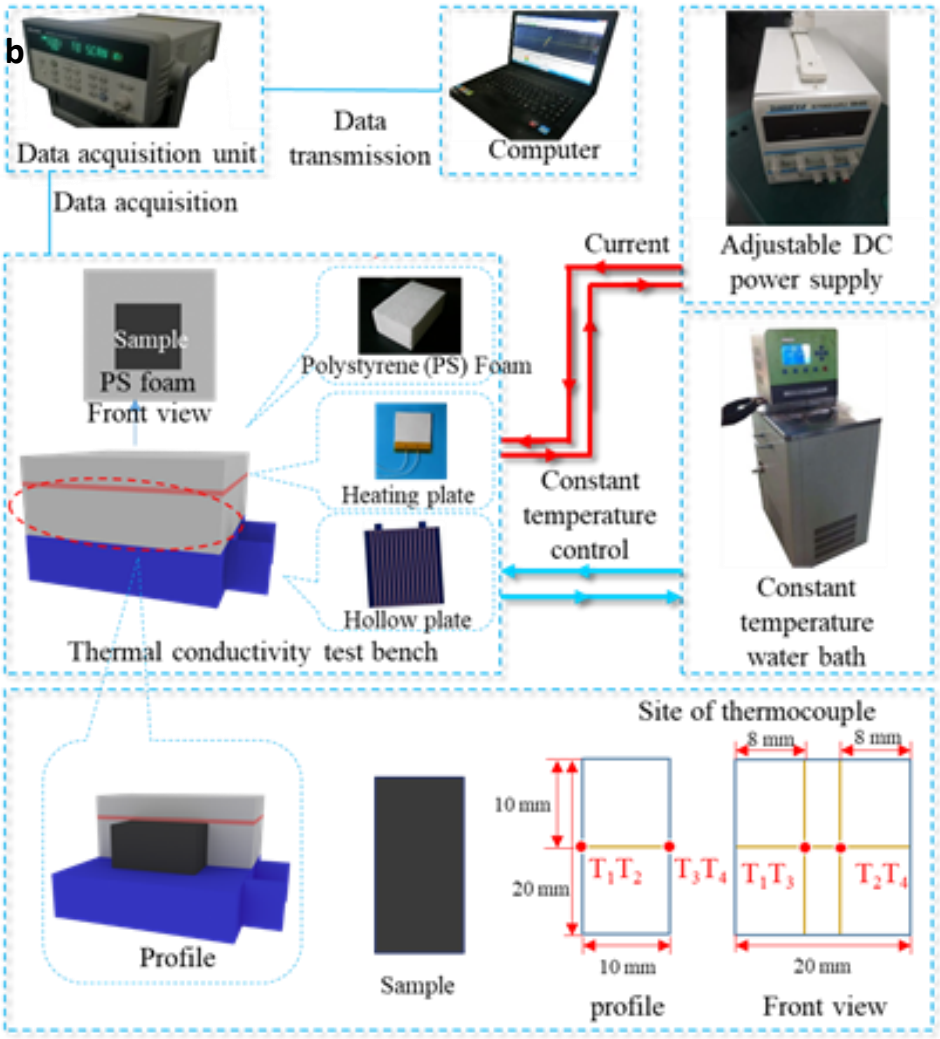

As the heterogeneous characteristic of the PCM composite, traditionally used thermal conductivity device that based on a transient plane source method is not suitable. In this work,the thermal conductivity of KAPs-CF-PCM composites was evaluated referring a literature[2] by placing the sample in between a hot and a cold plate and measuring the temperature gradient under varying heating power input (Q) with thermal couples on the basis of Fourier's law.

Table S2 Phase change temperature and latent heat of the as-prepared PCM composites.

Sample	Melting process			Freezing process		
	Onset (°C)	Peak (°C)	ΔH_m (J/g)	Onset (°C)	Peak (°C)	ΔH_f (J/g)
Paraffin	48.18	57.12	170.01	63.31	48.96	169.53
KAPs-CF-PCM (**1**)	50.28	57.20	70.94	53.59	48.76	70.85
KAPs-CF-PCM (2)	50.80	58.16	**105.60**	53.41	46.88	**105.98**
KAPs-CF-PCM (**3**)	49.95	56.29	68.67	53.48	49.96	68.36
KAPs-CF-PCM (**4**)	50.19	57.72	79.51	53.12	47.38	79.69
KAPs-CF-PCM (**5**)	49.41	56.74	74.28	52.95	47.76	74.29
KAPs-CF-PCM (**6**)	50.14	56.39	68.85	53.67	48.86	68.75
KAPs-CF-PCM (**7**)	49.53	54.83	64.76	53.40	50.21	64.32
KAPs-CF-PCM (**8**)	49.40	56.56	78.78	52.95	48.18	79.01
KAPs-CF-PCM (**9**)	50.22	56.84	96.40	53.48	48.44	93.26
KAPs-CF-PCM (**10**)	49.63	55.44	63.96	53.62	47.52	64.02
KAPs-CF-PCM (**11**)	50.34	55.41	55.96	53.28	48.68	52.02
KAPs-CF-PCM (**12**)	49.96	54.29	48.56	53.48	50.39	49.63
KAPs-CF-PCM (**13**)	49.98	55.08	35.32	53.69	50.38	36.98

Table S3 Literature survey of fabricated copper foam encapsulated PCM composite and compared them with this work.

Entry	Pretreatment of copper foam	PCM holding method	Thermal conductivity ($W \cdot m^{-1} \cdot K^{-1}$)	Latent heat (J/g)	Reference
1	Oxidation and polymer aided carbon coating	Vacuum impregnation	3.94	103.3	[2]
2	chemical-vapor deposited (CVD) multi-layer graphene	Vacuum impregnation	10.6	--	[3]
3	$FeCl_3$ immersion and vapor-phase polymerization in a pyrrole gas	Vacuum impregnation	98.1–126.4[a]	54.66	[4]
4	absorbent cotton sheet carbonized as carbon fiber frameworks	Vacuum impregnation	0.77	199.4	[5]
5	--	Impregnation at 120℃	2.14	151.6	[6]
6	--	--	3.8	--	[7]
7	--	Vacuum impregnation	4.9	132.5	[8]
8	--	Vacuum impregnation	1.45	94.33	[9]
9	--	--	3.92	--	[10]
10	--	--	0.82	--	[11]
11	SAT samples are modified by using DHPD and CMC	Impregnation	3.3-6.8	--	[12]
12	Thermal exfoliation of GO to make GS	Impregnation	3.55	250	[13]
13	CNF/GNP hybrid-coated MF	Vacuum impregnation	0.26	178.9	[14]

14	Ni foam filled with the Ni powder/PMMA and then covered with graphene	Vacuum impregnation	2.28	151.1	[15]
15	SA was dissolved in ethanol solution and then rGO@MOF-5-C was introduced into SA solution	Impregnation	0.60 ± 0.02	168.7	[16]
16	AgNP-decorated diatomite powder (denoted as DtAg)	Vacuum impregnation	0.82	--	[17]
17	fatty amines (FAs) filled porous 3D graphene sponge (GS)	Vacuum impregnation	0.3443-0.4944	293-303	[18]
18	graphene/paraffin aerogels	Vacuum impregnation	0.248	202.2	[19]
19	KAPs embedding method	Vacuum impregnation	55.0	105.6	This work

[a] Deduced data based on thermal effusivity.

Table S4 Literature survey on PCM shape-stabilization for thermal energy storage.

Author	Preparation method	Structure characterization							Thermo-physical properties					Real application				
		SEM	TEM	XRD	FTIR	TGA	XPS	N_2 adsorption curve	Pore size distribution	Thermal conductivity	Latent heat	Leakage proof	Mechanic study	Shape adjustability	Light-to-electric conversion	Light-to-thermal conversion	Thermal effusivity study	Heat sink	
Liu et al.	Vacuum impregnation	√	√	√	√	√	√	√	√	√	√	√	√	√	√	√	√	√	This work
Liu et al.[20]	In-situ polymerization	√	√	√	√	√	√	×	×	√	√	√	×	×	×	×	×	×	J. Mater. Chem. A
Ye et al[2]	Vacuum impregnation	√	×	×	√	√	√	×	×	√	√	√	√	×	√	√	×	×	ACS Appl. Mater. Inter.
Wu et al[14]	Vacuum impregnation	√	×	×	√	×	×	×	×	√	√	√	√	√	√	√	×	√	ACS Appl. Mater. Inter.
Lei et al[4]	Vacuum impregnation	√	×	×	√	√	×	×	×	√	√	√	×	×	×	×	√	×	J. Mater. Chem. A
Yang et al[21]	Vacuum impregnation	√	√	×	√	√	√	×	×	√	√	√	√	×	√	√	×	√	Nanoscale
Wei et al[22]	Sol-gel method	√	×	×	×	×	×	×	×	√	√	√	×	×	√	√	×	×	Green Chem.

Sheng et al[5]	Vacuum impregnation	√	√	√	×	√	×	×	×	√	√	√	√	√	×	×	×	×	J. Mater. Chem. A
Cottrill et al[3]	Vacuum impregnation	√	×	×	√	√	×	×	×	√	√	×	×	√	√	√	√	×	Nat. Commun.
Chen et al[18]	Melt impregnation	√	×	√	√	√	√	√	×	√	√	×	×	×	×	×	×	×	Chem. Eng. J.
Wu et al[23]	Diels–Alder reaction	√	×	√	√	√	×	×	×	√	√	√	√	√	×	×	×	×	J. Mater. Chem. A
Du et al[24]	Condensation reaction	√	×	×	√	√	×	×	√	√	√	×	×	×	×	×	×	×	J. Mater. Chem. A
Humphries et al[25]	Vacuum impregnation	√	×	×	√	√	×	×	×	√	√	×	√	√	×	×	×	×	J. Mater. Chem. A
Huang et al[26]	Phase change microcapsule	√	√	√	√	√	×	×	√	√	√	×	√	×	×	×	×	×	J. Mater. Chem. A
Tian et al[27]	Static melting method	√	√	×	√	√	×	×	×	√	√	×	×	×	×	×	×	×	J. Mater. Chem. A
Yang et al[28]	Solution blending method	√	√	√	√	√	√	×	×	√	√	√	×	√	√	√	×	×	J. Mater. Chem. A
Chen et al[29]	In-situ polymerization	√	×	√	√	√	×	×	×	√	√	√	√	√	×	×	×	×	J. Mater. Chem. A

Qian et al[17]	Vacuum impregnation	√	×	×	√	√	×	×	×	√	√	√	×	√	×	×	×	×	J. Mater. Chem. A
Luo et al[30]	Vacuum impregnation	√	×	×	√	√	×	×	×	√	√	√	×	×	√	√	×	×	J. Mater. Chem. A
Ye et al[19]	Sol-gel method	√	×	×	√	√	√	×	×	√	√	√	×	√	×	×	×	×	J. Mater. Chem. A
Huang et al[31]	Vacuum impregnation	√	×	√	√	√	×	×	√	√	√	√	×	√	√	√	×	×	J. Mater. Chem. A
Jing et al[32]	Vacuum impregnation	√	×	×	√	√	×	×	×	√	√	√	×	√	√	√	×	×	ACS Appl. Mater. Inter.
Li et al[16]	In-situ polymerization	√	×	√	√	√	×	√	×	√	√	×	×	×	×	×	×	×	ACS Appl. Mater. Inter.
Gros u et al[33]	Vacuum impregnation	√	×	√	√	√	×	×	×	√	√	×	×	×	√	√	×	×	ACS Appl. Mater. Inter.
Xin et al[13]	Vacuum impregnation	√	×	√	√	√	×	×	×	√	√	√	×	√	×	×	×	×	ACS Appl. Mater. Inter.
Liu et al [1]	In-situ polymerization	√	√	√	√	√	√	×	×	√	√	√	×	×	×	×	×	×	Int. J. Heat Mass Tran.
Zhang et al[34]	In-situ polymerization	√	×	√	√	√	×	×	×	√	√	×	√	√	×	×	×	×	J. Mater. Chem.
Yin et al[35]	In-situ polymerization	√	×	×	√	√	×	×	×	√	√	√	×	×	√	√	×	×	Int. J. Energ. Res.

Liang et al[36]	Vacuum impregnation	√	×	√	√	√	×	×	√	√	√	√	×	√	√	√	×	×	Chem. Mater.

Figure S9 Leakage-proof performance of KAPs-CF-PCM (x), the samples were placed on a filtration paper and heated in a 80 ºC oven, the leakage images were recored by a digital camera in a 5 min interval.

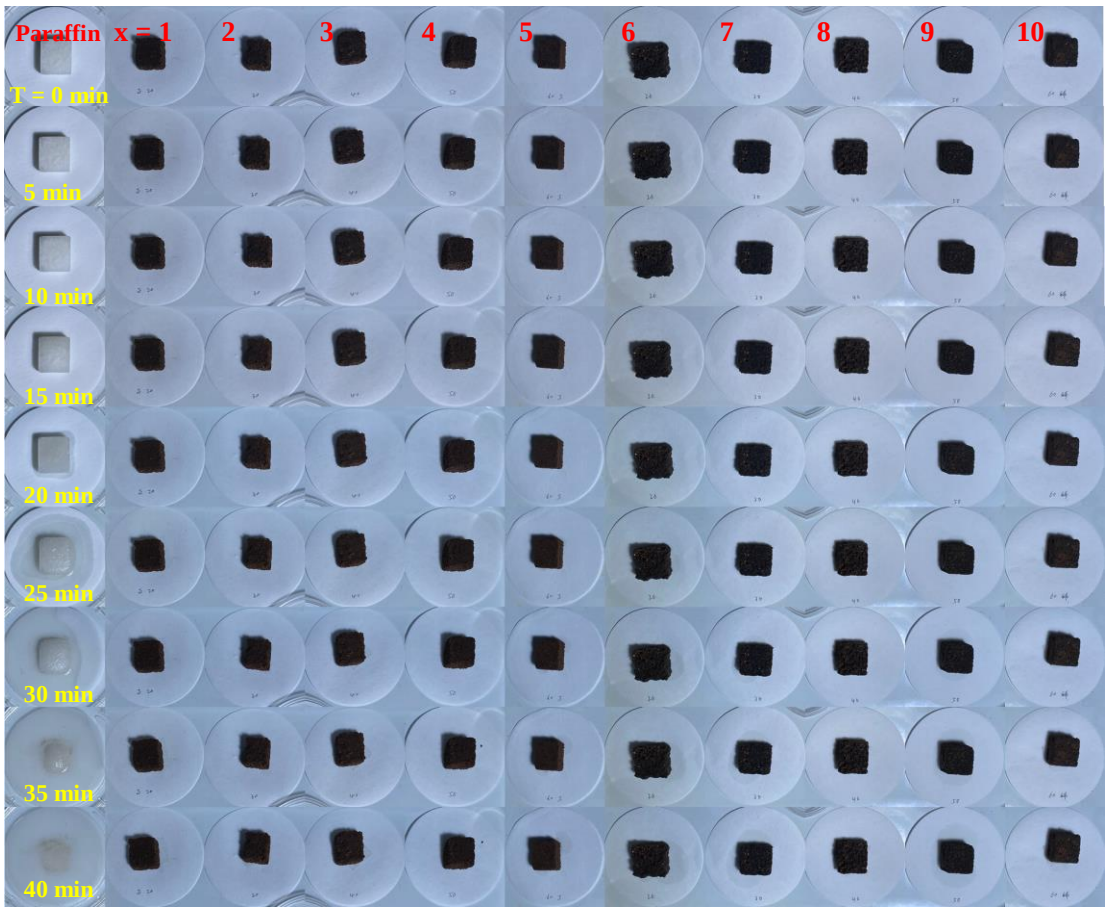

Figure S10 Mechanical properties study on KAPs-CF-PCM.

Figure S11 Photograph of light-to-thermal conversion performance testing platform

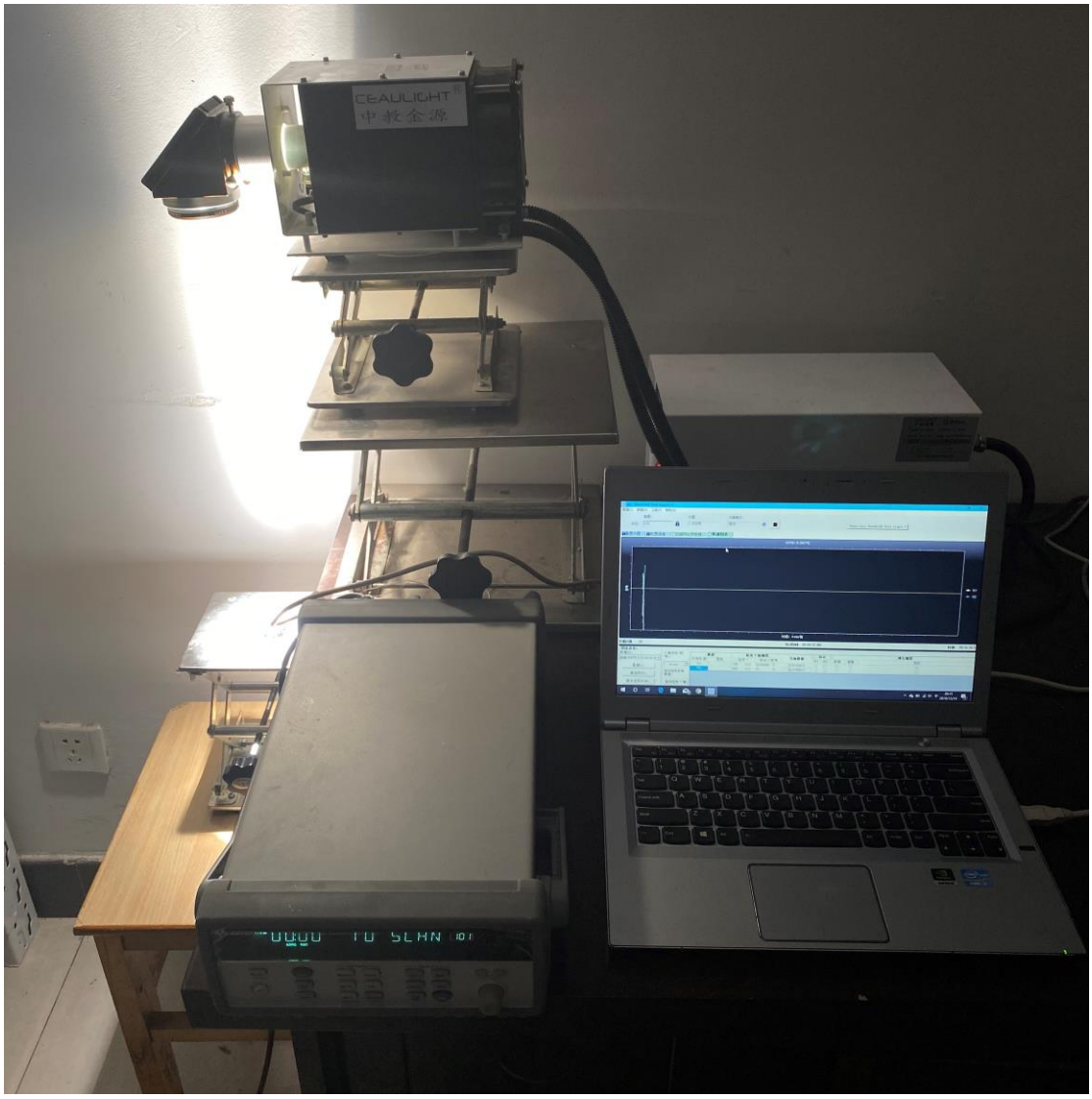

Figure S12 Photograph of light-to-electric conversion performance testing platform.

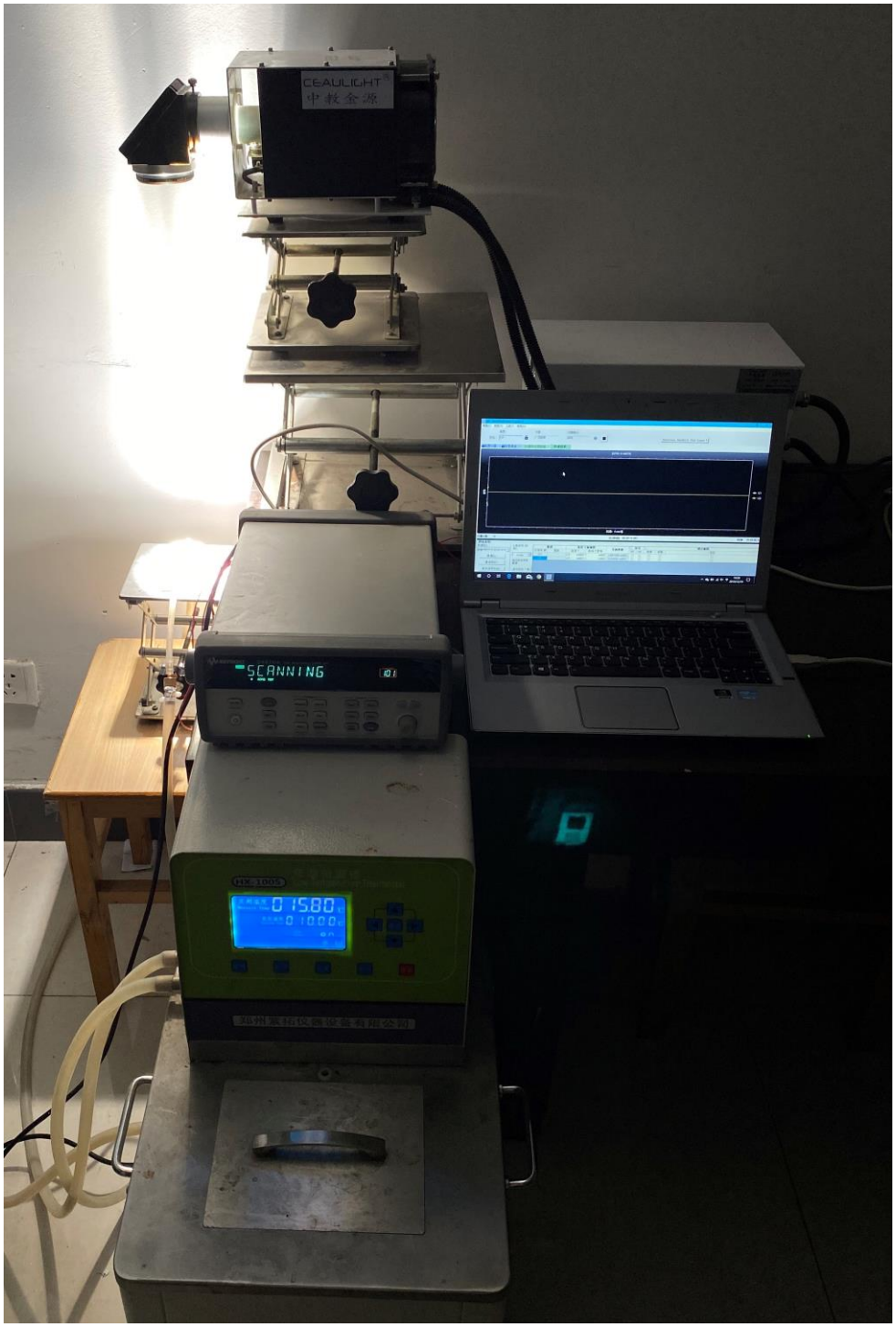

Reference

1. C. H. Liu, Y. Song, Z. Xu, J. T. Zhao and Z. H. Rao, *International Journal of Heat and Mass Transfer*, 2020, **148**, 11.
2. Q. Ye, P. Tao, C. Chang, L. Zhou, X. Zeng, C. Song, W. Shang, J. Wu and T. Deng, *ACS Appl Mater Interfaces*, 2019, **11**, 3417-3427.
3. A. L. Cottrill, A. T. Liu, Y. Kunai, V. B. Koman, A. Kaplan, S. G. Mahajan, P. Liu, A. R. Toland and M. S. Strano, *Nat Commun*, 2018, **9**, 664.
4. H. Lei, C. Fu, Y. Zou, S. Guo and J. Huo, *Journal of Materials Chemistry A*, 2019, **7**, 6720-6729. (41)
5. N. Sheng, R. Zhu, K. Dong, T. Nomura, C. Zhu, Y. Aoki, H. Habazaki and T. Akiyama, *Journal of Materials Chemistry A*, 2019, **7**, 4934-4940.
6. P. Chen, X. N. Gao, Y. Q. Wang, T. Xu, Y. T. Fang and Z. G. Zhang, *Solar Energy Materials and Solar Cells*, 2016, **149**, 60-65.
7. S. Thapa, S. Chukwu, A. Khaliq and L. Weiss, *Energy Conversion and Management*, 2014, **79**, 161-170.
8. X. Xiao, P. Zhang and M. Li, *Applied Energy*, 2013, **112**, 1357-1366.
9. X. Huang, Y. Lin, G. Alva and G. Fang, *Solar Energy Materials and Solar Cells*, 2017, **170**, 68-76.
10. S. Feng, Y. Zhang, M. Shi, T. Wen and T. J. Lu, *Applied Thermal Engineering*, 2015, **88**, 315-321.
11. W. Q. Li, Z. G. Qu, Y. L. He and Y. B. Tao, *Journal of Power Sources*, 2014, **255**, 9-15.
12. T. X. Li, D. L. Wu, F. He and R. Z. Wang, *International Journal of Heat and Mass Transfer*, 2017, **115**, 148-157.
13. G. Xin, H. Sun, S. M. Scott, T. Yao, F. Lu, D. Shao, T. Hu, G. Wang, G. Ran and J. Lian, *ACS Appl Mater Interfaces*, 2014, **6**, 15262-15271.
14. H. Wu, S. Deng, Y. Shao, J. Yang, X. Qi and Y. Wang, *ACS Appl Mater Interfaces*, 2019, **11**, 46851-46863.
15. G. Qi, J. Yang, R. Bao, D. Xia, M. Cao, W. Yang, M. Yang and D. Wei, *Nano Research*, 2016, **10**, 802-813.
16. A. Li, C. Dong, W. Dong, D. G. Atinafu, H. Gao, X. Chen and G. Wang, *ACS Appl Mater Interfaces*, 2018, **10**, 32093-32101.
17. T. Qian, J. Li, X. Min, W. Guan, Y. Deng and L. Ning, *Journal of Materials Chemistry A*, 2015, **3**, 8526-8536.
18. T. Chen, C. Liu, P. Mu, H. Sun, Z. Zhu, W. Liang and A. Li, *Chemical Engineering Journal*, 2020, **382**.
19. S. Ye, Q. Zhang, D. Hu and J. Feng, *Journal of Materials Chemistry A*, 2015, **3**, 4018-4025.
20. C. Liu, Z. Xu, Y. Song, P. Lv, J. Zhao, C. Liu, Y. Huo, B. Xu, C. Zhu and Z. Rao, *Journal of Materials Chemistry A*, 2019, **7**, 8194-8203.
21. J. Yang, P. Yu, L. S. Tang, R. Y. Bao, Z. Y. Liu, M. B. Yang and W. Yang, *Nanoscale*, 2017, **9**, 17704-17709.
22. Y. H. Wei, J. J. Li, F. R. Sun, J. R. Wu and L. J. Zhao, *Green Chem.*, 2018, **20**, 1858-1865.
23. B. Wu, Y. Wang, Z. Liu, Y. Liu, X. Fu, W. Kong, L. Jiang, Y. Yuan, X. Zhang and J. Lei, *Journal of Materials Chemistry A*, 2019, **7**, 21802-21811.
24. X. Du, S. Wang, Z. Du, X. Cheng and H. Wang, *Journal of Materials Chemistry A*, 2018, **6**, 17519-17529.
25. T. D. Humphries, D. A. Sheppard, G. Li, M. R. Rowles, M. Paskevicius, M. Matsuo, K.-F. Aguey-

Zinsou, M. V. Sofianos, S.-i. Orimo and C. E. Buckley, *Journal of Materials Chemistry A*, 2018, **6**, 9099-9108.

26. Y. T. Huang, H. Zhang, X. J. Wan, D. Z. Chen, X. F. Chen, X. Ye, X. Ouyang, S. Y. Qin, H. X. Wen and J. N. Tang, *Journal of Materials Chemistry A*, 2017, **5**, 7482-7493.
27. H. Q. Tian, L. C. Du, C. L. Huang, X. L. Wei, J. F. Lu, W. L. Wang and J. Ding, *Journal of Materials Chemistry A*, 2017, **5**, 14811-14818.
28. J. Yang, G. Q. Qi, L. S. Tang, R. Y. Bao, L. Bai, Z. Y. Liu, W. Yang, B. H. Xie and M. B. Yang, *Journal of Materials Chemistry A*, 2016, **4**, 9625-9634.
29. Z. Chen, J. Wang, F. Yu, Z. Zhang and X. Gao, *Journal of Materials Chemistry A*, 2015, **3**, 11624-11630.
30. W. Luo, Y. Feng, C. Cao, M. Li, E. Liu, S. Li, C. Qin, W. Hu and W. Feng, *Journal of Materials Chemistry A*, 2015, **3**, 11787-11795.
31. X. Huang, Z. Liu, W. Xia, R. Zou and R. P. S. Han, *Journal of Materials Chemistry A*, 2015, **3**, 1935-1940.
32. J.-h. Jing, H.-y. Wu, Y.-w. Shao, X.-d. Qi, J.-h. Yang and Y. Wang, *ACS Applied Materials & Interfaces*, 2019, **11**, 19252-19259.
33. Y. Grosu, M. Mierzwa, V. A. Eroshenko, S. Pawlus, M. Chorazewski, J. M. Nedelec and J. E. Grolier, *ACS Appl Mater Interfaces*, 2017, **9**, 7044-7049.
34. X. H. Zhang, L. Zhu, Y. L. Dong, W. J. Weng, G. R. Han, N. Ma and P. Y. Du, *J. Mater. Chem.*, 2010, **20**, 10856-10861.
35. D. Z. Yin, L. Ma, W. C. Geng, B. L. Zhang and Q. Y. Zhang, *International Journal of Energy Research*, 2015, **39**, 661-667.
36. X. Liang, V. Kozlovskaya, Y. Chen, O. Zavgorodnya and E. Kharlampieva, *Chem. Mat.*, 2012, **24**, 3707-3719.